Journal of Power Sources 184 (2008) 353–360

Contents lists available at ScienceDirect

Journal of Power Sources

journal homepage: www.elsevier.com/locate/jpowsour

Size-effect on the activity of anodic catalysts in alcohol and CO electrooxidation

Xiaoxia Li, Xinping Qiu*, Huiping Yuan, Liquan Chen, Wentao Zhu

Key Laboratory of Organic Optoelectronics and Molecular Engineering, Department of Chemistry, Tsinghua University, Beijing 100084, China

ARTICLE INFO

Article history:
Received 8 January 2008
Received in revised form 14 March 2008
Accepted 17 March 2008
Available online 29 March 2008

Keywords:
Size-effect
Catalytic activity
CO electrooxidation
Alcohol electrooxidation

ABSTRACT

The aim of this report is to investigate the particle size-effect of Pt on the catalytic activities for high surface area catalysts. Series of Pt/MWCNTs catalysts with average particle size of 1.7, 2.4, and 4.0 nm were fabricated. Size-effect on their catalytic activity towards CO as well as alcohol electrooxidation reactions was studied by CO-stripping, cyclic voltammetry, and chronoamperometry. We for the first time investigated the size-effect on the apparent activation energy for the reaction of CO electrooxidation. The results showed that the catalytic activities had a strong dependence on their Pt particle size. (1) The reaction of CO electrooxidation on the smaller Pt nanoparticles was found occurring at the higher overpotential and apparent activation energy than on the larger counterparts. The intrinsic nature of those observed phenomena were due to the stronger CO adsorption on the smaller Pt nanoparticles. (2) As the size decreased, the mass activity towards alcohol electrooxidation increased; considering the discount of this increase for the smaller particles, we concluded that the deactivation arising from their more intense CO-poisoning, which limited the beneficial effect on their higher mass activity in this case.

1. Introduction

Extensive research into direct alcohol fuel cells (DAFCs) is connected to the worldwide demand for the sustainable energy. Up to now, prohibitively high cost of noble Pt catalysts is still the main limitation for its application. Regarding the anodic catalysts, the activity of carbon supported Pt-based catalysts is definitely required to be improved in order to promote their efficiency of delivering chemical energy into electricity as well as to reduce their cost [1–3]. Thus, intensive research works have been dedicated to prepare the catalyst with high activity. Meanwhile, the experiments were in part designed to examine the influential factors to their activities and to develop an in-depth understanding for their intrinsic catalytic nature.

Both of alcohol and CO electrooxidation are structure-sensitive reactions. According to the literatures, several factors had significant influence on the activity of the anodic catalysts, including the catalyst support [4,5], the morphology of Pt nanoparticles [6], and the average size of Pt particles [7–11]. Among them, the study of size-effect on catalytic properties was performed and demonstrated some interesting results. For the process of CO electrooxidation, different groups studied the particle size influence and tried to reveal the intrinsic nature of the catalysts. They achieved similar results but provided different explanations. Maillard et al. reported a positive shift of CO-stripping peak as the size of Pt decreased from 4 to 1 nm. They attributed the low activity on small Pt particles to the low mobility of CO_{ads} on their surface through a mathematic modeling fitting [7]. Arenz et al. showed that the rate of CO_2 production is strongly depended on the size of Pt nanoparticles with an order of $1 \leq 2 < 5 \ll 30$ nm. However, they ascribed their results to the number of defects, which were abundant on the surface of large particles and played a beneficial role in CO oxidative removal [8].

Apart from the size-effect on CO electrooxidation, size-effect towards methanol electrooxidation was also examined by several research groups but illustrated different complicated results [9–11]. Bergamaski et al. [9] found that an optimum particle size for electrooxidation methanol to CO_2 was 3–10 nm, and the loss in efficiency mostly occurred on either too small or too large particles. In the case of the particle size below 5 nm, Tang et al. [10] reported that the mass activity (MA, per unit weight of Pt) of methanol electrooxidation increased as the particle size increased from 2.2 to 3.8 nm but decreased as the particle size further increased to 4.3 and 4.8 nm. However, Zeng et al. [11] showed that the mass activity decreased monotonously as the particle size increased from 2.2 to 4.0 nm, although the change of specific activity (SA, per unit electroactive surface area of Pt) showed an opposite trend.

Activity investigations towards CO electrooxidation and alcohol electrooxidation are the two main aspects to evaluate the activity of the anodic catalysts in DAFC. The results of the former can help us understand the intrinsic catalytic nature and the latter one can give us directly the activity performance of the catalysts and the

* Corresponding author. Tel.: +86 10 62794234; fax: +86 10 62794234.
E-mail address: qiuxp@tsinghua.edu.cn (X. Qiu).

0378-7753/$ – see front matter © 2008 Elsevier B.V. All rights reserved.
doi:10.1016/j.jpowsour.2008.03.058

effectiveness of Pt utilization. However, as the particle size of Pt decreased below 5 nm, research works related to the relationship between alcohol electrooxidation and CO electrooxidation are still very limited.In our approach, we prepared series of Pt/MWCNTs catalysts as Pt particles were deposited in a mono-dispersed form on the same support with same prepared method. In the case of eliminating all other influential factors, we studied only size-effect on the catalytic activity both towards CO electrooxidation and alcohol electrooxidation reactions and expected to gain a better insight into the overall of size-effect.

2. Experimental

2.1. Preparation and characterization of the catalysts

Series of catalysts Pt/MWCNTs with different size of Pt nanoparticles were fabricated. The process of the catalyst fabrication was illustrated in Scheme 1. Before depositing Pt on the MWCNTs, the MWCNTs were treated with a microwave assistant process to improve their hydrophilicity and dispersion in aqueous solution by generating some oxygenic species on their surface [12]. In detail, the raw MWCNTs was ultrasonically radiated for 1 h in a mixture solution of 98% H_2SO_4/65% HNO_3 (1:1, v/v), then the microwave treatment followed for 3 min in air (for the safety reason, the microwave oven should be placed in a fume hood and the treatment must be carefully conducted!). They are ready for use after rinsed several times with deionized water. The sizes of Pt particles were controlled via the polyol process by changing the concentration of NaOH in ethylene glycol solution [13]. Typically, MWCNT was ultrasonically treated in ethylene glycol solution of NaOH for 1 h, wherein a calculated amount of hexachloroplatinic acid (dissolved in ethylene glycol) was dropped, and then the mixture was refluxed at 140 °C for 3 h under stirring. After filtrated, rinsed and dried, the catalysts of Pt/MWCNTs were fabricated. In our approach, we tried three various concentration of NaOH (0, 0.01, and 0.1 M) and obtained three samples assigned as A, B, and C, respectively. Commercial Pt/C (E-Tek Pt: 20 wt%) was studied in parallel as a benchmark and assigned as sample D.

The XRD patterns of the as-prepared products were investigated via a Bruker powder diffraction system (model D8 Advanced), using Cu Kα as the radiation source at the operating voltage of 40 kV and a scan rate of 6° min^{-1}. The size and the dispersion of Pt nanoparticles were observed using high-resolution transmission electron microscopy (HRTEM, Tecnai G2 F20 S-Twin) at 200 kV. And the average size of Pt was calculated from the size distribution of 100 nanoparticles in TEM images. The X-ray photoelectron spectroscopic (XPS) analysis was carried out to study the valence state of Pt with a Physical Electronics PHI Quantera SXM system (PHI 5300, ULVAC-PHL, Inc.) using an Al monochromatic X-ray source. To compensate for surface charges effects, binding energies were calibrated using C 1s hydrocarbon peak at 284.8 eV. The compositions of the catalysts were investigated using an energy dispersive X-ray spectrometer (EDS, Oxford Instrument) attached to the scanning electron microscopy (SEM, JSM-6301F) at 15 kV. In EDS investigation, at least three measurements were conducted for each sample to calculate the average composition. Typically, a sample area of ca. 1 μm × 1 μm was scanned for at least 200 s to control the quantitative error in a minor level.

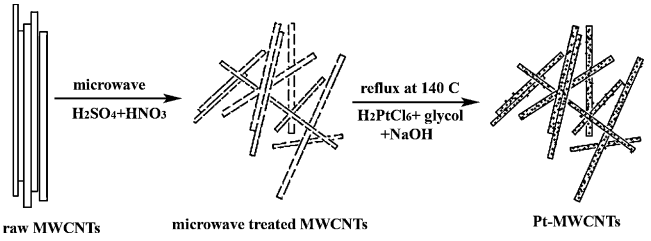

Scheme 1. The typical process of fabricating the catalyst of Pt/MWCNTs.

2.2. Electrochemical assessments

A planar gold patch (1.2 cm × 1.2 cm) coating with the catalyst ink was used as the working electrode. The fabrication of working electrode is same to the procedure of our previous work [3]. Electrochemical measurements were conducted on a potentiostat (EG&G Princeton, model 2273A). A Pt foil (1.2 cm × 1.2 cm) and a saturated calomel electrode (SCE) were used as the counter and the reference electrode, respectively. In a conventional, three-electrode cell, the reference electrode was placed in a separate chamber, located near the working electrode through a Luggin capillary tube. All potentials presented in this study were quoted with respect to SCE.

CO-stripping voltammetry was performed and the charge of CO-stripping was used to calculate the electroactive surface area (ESA, $m^2\,g^{-1}$) of Pt particles, assuming that the charge of 420 μC per 1 cm^2 of Pt was required to remove the adsorbed monolayer of CO [14,15]. The process was similar to our previous work [3]. The peak potentials of CO oxidation (E_p) were found to be the linear function of the absolute temperature (T) [16], and the relationship between E_p and T can be expressed as a straight line in a particular temperature range. From the intercept of the line, we can calculate the apparent activation energy of the reaction. In order to obtain the value, all of potentials were converted to a common standard hydrogen electrode at 298 K (SHE, 298 K) according to Eqs. (1) and (2):

$$E_{SHE,T} = E_{SCE,T} + 0.2412\,V \quad (1)$$

$$E_{SHE,298} = E_{SHE,T} + (T - 298)\frac{\partial E}{\partial T} \quad (2)$$

$\partial E/\partial T$ has the value of $8.4 \times 10^{-4}\,V\,K^{-1}$. Herein, the size-effect on the function of E_p and T was studied for the first time to compare the apparent activation energy on different size of Pt catalysts. The experiments for samples A and C were performed at 25, 35, 45, 55, and 65 °C by immersing the three-electrode cell in a water bath as the counter and reference electrodes maintained at the same temperature as the working electrode (SCE, T). The temperatures were controlled to within 0.5 K.

The particle size-effect on the activity towards alcohol electrooxidation was investigated by potentiodynamic (cyclic voltammogram, CV) and potentiostatic assessments (chronoamperometry) for the series of Pt/MWCNT catalysts. The peak currents were normalized by the weight of Pt to illustrate directly the size-effect on MA (mA mg^{-1} Pt). The measurements were repeated at least three times for each catalyst and mean values of MA are reported here. The values of SA (mA cm^{-2} Pt) were also calculated correspondingly to evaluate the size-effect on the intrinsic catalytic nature from another aspect.

3. Results and discussions

3.1. The structure characterization

Fig. 1 demonstrates typical TEM, HRTEM images and the histogram of size distribution for sample A. It can be seen that Pt nanoparticles deposited in a highly dispersed form on the surface of MWCNTs (Fig. 1a). Fig. 1b is the magnified TEM images, and the inset is the HRTEM image of Pt nanoparticles. It can also be seen that Pt particles normally have spheroid shape. The lattice

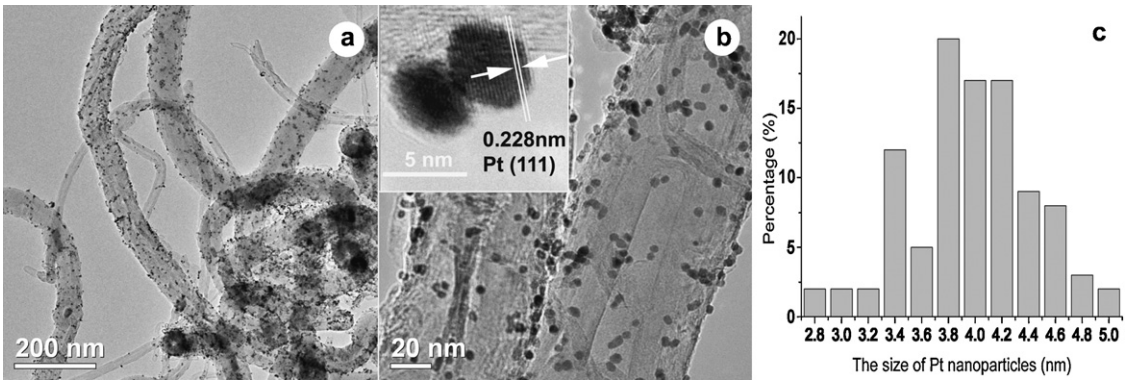

Fig. 1. The typical (a) TEM image, (b) magnified TEM image, and (c) the histogram of size distribution for sample A. The inset of (b) is the HRTEM image of Pt nanoparticles, from which the crystal lattice of (1 1 1) planes of Pt can be observed clearly, indicating the good crystallization of Pt.

fringe separation is observed to be 0.228 nm, which is attributed to the corresponding (1 1 1) planes and consistent with the results obtained from XRD diffractions (see the following discussion), suggesting the good crystallization of Pt. The size distribution of Pt particles is narrow and the size (90%) was found in the range of 4.0 ± 0.6 nm (from Fig. 1c) with the average size of 4.0 nm.

Similarly, Figs. 2 and 3 demonstrates typical TEM, HRTEM images and the histograms of size distribution for samples B and C, respectively. It can be seen that Pt nanoparticles in two samples are also spheroid and highly dispersed on the surface of MWCNTs. The size of Pt particles (90%) was found in the range of 2.4 ± 0.6 nm for sample B, and 1.7 ± 0.7 nm for sample C. The results confirmed that the concentration of NaOH actually play an important role in controlling the size of metal via the polyol process [13], as the size of Pt particles was found decreased along with the concentration of NaOH increased. Although the size for samples B and C decreased dramatically in comparison with sample A, the crystallization of Pt was not affected by the increased concentration of NaOH. The crystal lattice of Pt (1 1 1) planes can also be observed clearly from the inset HRTEM images in Figs. 2b and 3b. Typically, the low-index planes were observed governing the surface of Pt particles for three samples, indicating that the Pt nanoparticles prepared by polyol process are mainly enclosed by the low-index planes. Furthermore, the low-index planes are terminated in an irregular way in the surfaces and cause the particles have nearly rounded or spheroid shape, rather than a perfect octahedron or cubic shape. This is consistent to the results of Tong's group [17] that there are particle size limit for concomitant tuning of size and shape of plat-

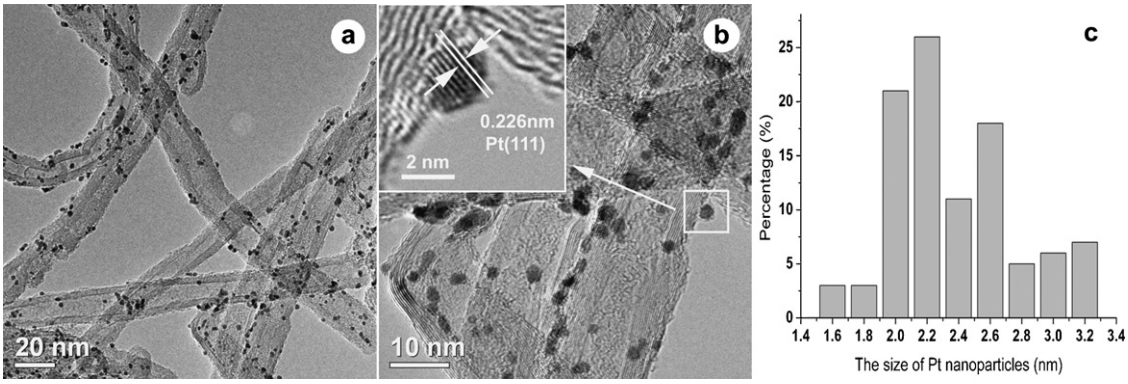

Fig. 2. As in Fig. 1 but for sample B.

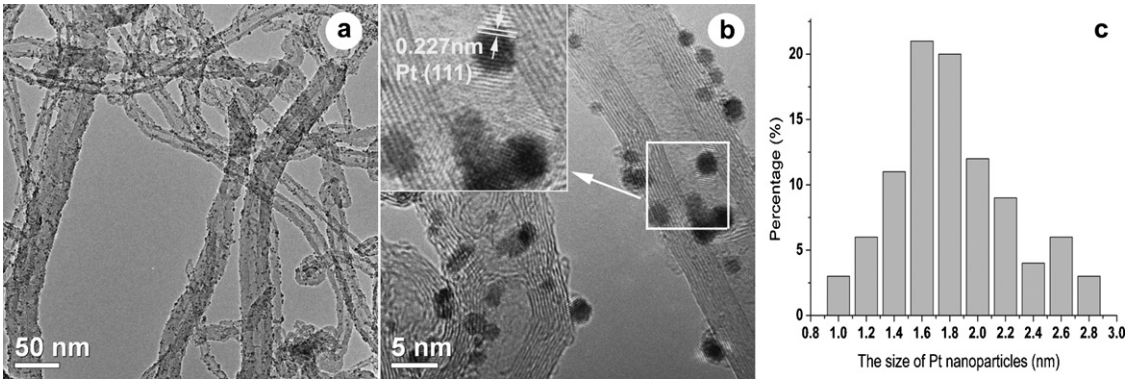

Fig. 3. As in Fig. 1 but for sample C.

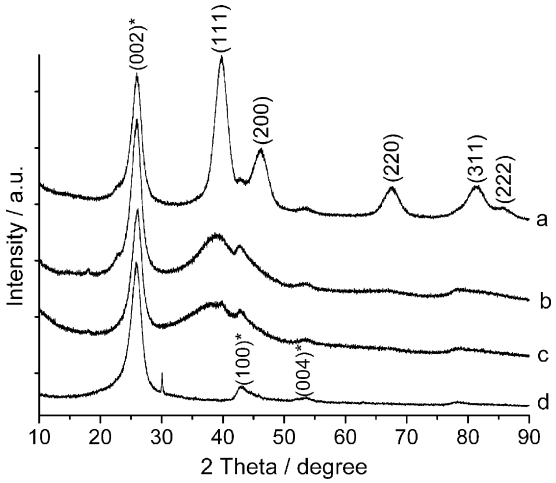

Fig. 4. Typical XRD patterns of (a) sample A, (b) sample B, (c) sample C, and (d) the support of MWCNTs. The diffraction peaks near 26.1°, 42.6°, and 54.0° are the representative peaks (0 0 2), (1 0 0), and (0 0 4) of graphite.

inum nanoparticles in polyol process. The spheroid shape is expect to provide more defects than perfect octahedron one and will play a crucial role in their catalytic activities. For the sample D, Pt particle size (90%) was found in range of 2.6 ± 0.7 nm with a mean size of 2.6 nm (not shown), which is consistent to the observation in Ref. [18].

The structure of the as-prepared samples A, B, and C was further studied by XRD, as shown in Fig. 4a–c. Fig. 4d is the diffraction pattern of the support MWCNTs for comparison. The existence of diffraction peaks at 26.1°, 42.6°, and 54.0° in all of patterns are the representative peak (0 0 2), (1 0 0), and (0 0 4) of graphite, respectively. The pattern of sample A exhibits the typical diffraction peaks (1 1 1), (2 0 0), (2 2 0), and (3 1 1) of Pt at 2θ values of 39.8°, 46.2°, 67.5°, and 81.4°, indicating the face-centered cubic (fcc) structure of Pt. In the typical patterns of samples B and C, however, only broaden peak (1 1 1) of Pt can be discerned. The other peaks appear broaden with the low intensity, which is due to the decreased size of Pt. The study of diffraction peaks is in agreement with the HRTEM observations, suggesting that the surface of Pt nanoparticles was enclosed by low-index planes with no preferred orientations.

XPS was used to identify different oxidation states of Pt, as demonstrated in Fig. 5. The Pt 4f region shows two doublets from the spin–orbital splitting of the $4f_{7/2}$ and $4f_{5/2}$ states, which appeared at ca. 71.6–72.0 and 75.0–75.3 eV, respectively. The lines can be deconvoluted into two pairs of overlapping peaks at 71.6, 72.9 eV and 75.0, 76.3 eV. These two pairs of peaks indicated that Pt is present in two different oxidation states, Pt^0 and Pt^{II}. Table 1 displayed the relative intensity of Pt^0 and Pt^{II} species, calculated from the relative intensities of two deconvoluted peaks for Pt $4f_{7/2}$. The amount of Pt^{II} species is found increased of 5% as platinum particle size decreased from 4.0 to 1.7 nm, revealing that smaller particles are easily oxidized [10]. With platinum particle size decreasing, the binding energies were observed shift to the slight high values [19].

Table 1
The relative intensity of Pt^0 and Pt^{II} species in Pt/MWCNTs catalysts A, B, and C

Sample	Relative intensity of Pt^0 (%)	Relative intensity of Pt^{II} (%)
A (4.0 nm)	79.7	20.3
B (2.4 nm)	78.9	21.1
C (1.7 nm)	74.0	26.0

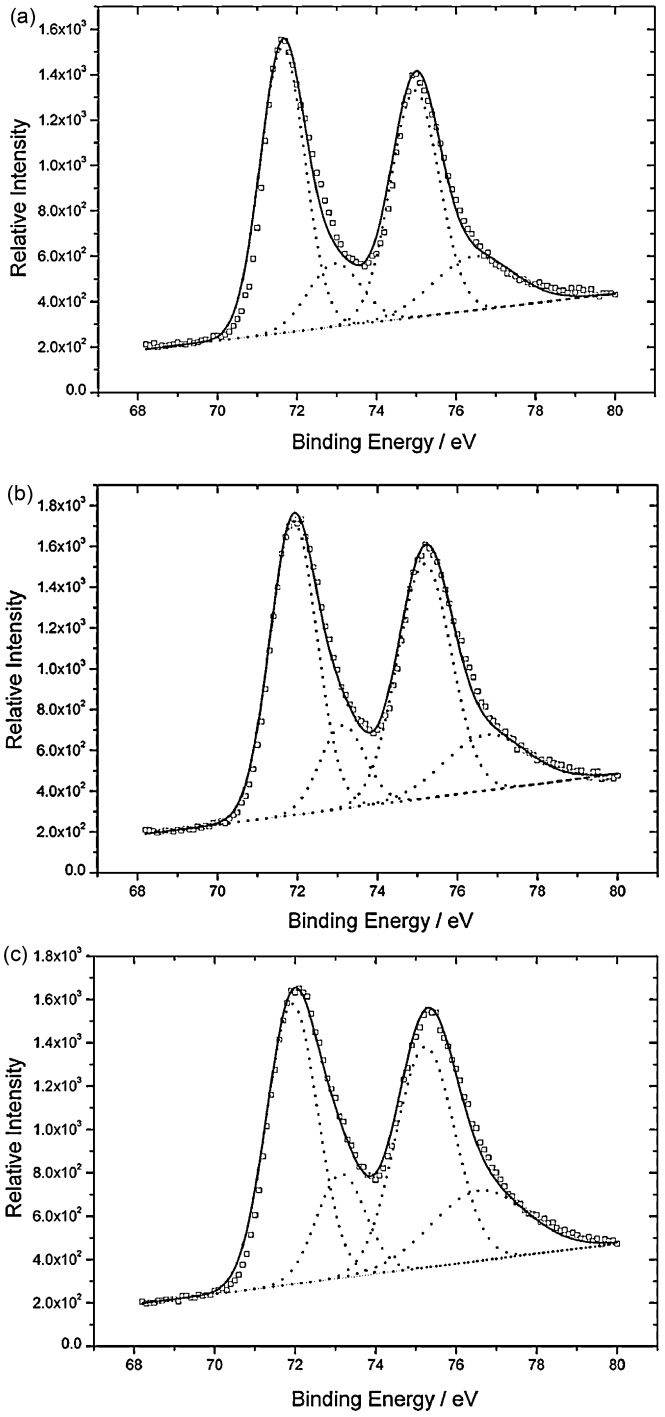

Fig. 5. The Pt 4f XPS spectra of the Pt/MWCNTs catalysts for (a) sample A, (b) sample B, and (c) sample C.

For the high-dispersed Pt nanoparticles in samples A, B, and C, the weight content of Pt were investigated by EDS and found to be 17.8%, 13.5%, and 13.6%, respectively.

3.2. Electrochemical properties and studies

It is well known that the active sites of Pt are prone to be poisoned by adsorbing intermediate CO and forming $Pt–CO_{ads}$ during the electrooxidation of primary alcohol. The reaction of CO electrooxidation on the anode is usually studied by CO-stripping.

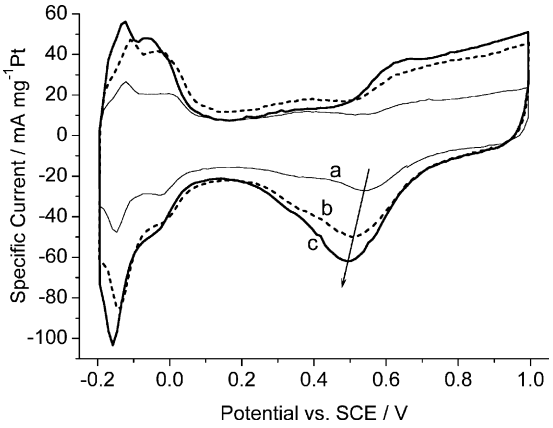

Fig. 6. The typical cyclic voltammogram curves for (a) sample A (light solid line), (b) sample B (dash line), and (c) sample C (solid line) in 1 M $HClO_4$ aqueous solution. After the curve reached stable, only the 50th cycle ones are demonstrated here.

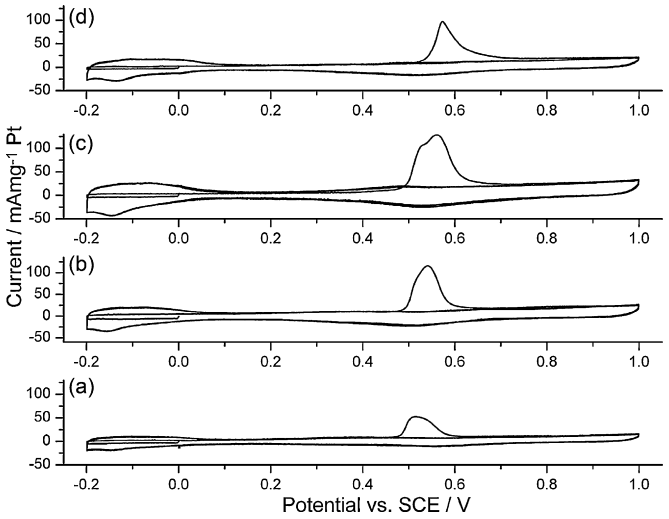

Fig. 7. CO-stripping curves for (a) sample A, (b) sample B, (c) sample C, and (d) sample D at 25 °C.

Before we discuss the curves of CO-stripping, it is appropriate for us to study the nature of catalysts A, B, and C through the cyclic voltammograms in the absence of CO, as shown in Fig. 6. There was no well-developed $H_{ads/des}$ peaks appeared in the first several cycles (not shown for clarity). As the scan going, typical feature of $H_{ads/des}$ with two pair peaks can be observed stable in the potential region of −0.2 to +0.1 V vs. SCE for three catalysts. The charges of $H_{ads/des}$ increased remarkably as the size decreased, indicating the increased ESA of the smaller particle catalyst. The potential range of above 0.5 V vs. SCE is the OH adsorption and oxide formation region. It can be seen that more OH species formed on per weight of smaller particles. According to the well-accepted Langmuir–Hinshelwood mechanism assumed for CO oxidation [20]:

$$C{\equiv}O_{ads} + OH_{ads} \rightarrow CO_2 + H^+ + e^- \quad (3)$$

More generated OH_{ads} on smaller Pt particles are expected to quantitatively beneficial to the reactions of CO electrooxidation and alcohol electrooxidation. In the back sweep, the potential of oxide reduction shifted negatively to a lower position for the smaller particles, reflecting the increased interaction between OH_{ads} and smaller Pt particles, which was explained due to the improved oxophilicity of the smaller particles by Arenz et al. [8].

The ESA of platinum can be calculated via CO-stripping charges, as shown in Fig. 7. The values for samples A, B, C, and D were figured out to be 37.9, 73.2, 107, and 61.9 $m^2\,g^{-1}$, respectively, which were a little lower than the corresponding values of 41.2, 81.5, 115, and 71.4 $m^2\,g^{-1}$, calculated from the H desorption charges after double layer correction in voltammetric curves. The origin of the increased ESA from samples A to C (except sample D) is reasonably due to the reduced particle size, which is also in line with the increased amount of OH_{ads} for per weight of smaller particles.

E_p for CO electrooxidation is observed at 0.516, 0.541, and 0.562 V for samples A, B, and C, respectively. E_p shifted remarkably to the high position as the size decreased, along with the peak width becoming large. It is in agreement with the results for Pt/GC electrode studied by Maillard et al. [7]. The positive shift was suggested due to the restricted CO-mobility on smaller particles by Maillard et al. [7] or due to the stronger adsorption of CO on smaller particles by Mukerjee and McBreen [21]. Besides, the interaction between Pt and OH_{ads} was also observed increased as the size decreased. Thus, we attributed the positive E_p shift to the combined roles of increased bond strength of Pt–CO_{ads} and Pt–OH_{ads} on smaller platinum particles, and the E_p of CO_{ads} electrooxidation is commonly regarded as a reflection of the bond strength of Pt–CO_{ads} and Pt–OH_{ads} on the anode. Those induced the overall CO_{ads} oxidation occurred at higher overpotential on smaller platinum particles. Moreover, we noticed that the peak profiles of CO electrooxidation on single crystal surface of Pt (1 1 1) and Pt (1 0 0) are sharper than that of Pt nanoparticles. We proposed that CO adsorption energies on the nearly perfect surface of Pt (1 1 1) or Pt (1 0 0) are almost uniform. On the contrary, the wide peak of Pt nanoparticles suggests that the CO adsorption energies on their round surface are in a wide distribution. The various adsorption energies are generated from their various low-index planes, which are abundant in different defects.

The onset and peak potentials for MWCNT supported samples are observed at lower positions than that of carbon-black supported sample D (E_p = 0.574 V). Considering that Pt size in sample C (1.7 ± 0.7 nm) is less than that of sample D (2.6 ± 0.7 nm), the negative instead of the positive E_p shift of sample C was not due to size-effect but due to the beneficial role of the MWCNT support [3]. Typically, the one-dimensional support can build a microporous catalytic layer, which facilitates the mass transport of the reactants and the product of CO_2, and therefore benefits the reaction of CO oxidation.

Apart from size-dependent behavior at 25 °C, E_p for CO electrooxidation was also reported to be temperature-dependent [16,22,23]. To the best of our knowledge, the size-effect on E_p shift under different temperatures has rarely been studied. Herein, the influence of temperature variation on E_p shift was examined in a comparing way for catalysts A and C for the first time. Since E_p is sensitive to the subtle variation of temperature and the layer microstructure of electrode, the experiments were repeated three times to reduce the experimental error. The mean values of E_p were found linear to T and their correlation could be fitted to be a straight line, as shown in Fig. 8. The function between E_p and T is expressed with Eqs. (4) and (5) for samples A and C, respectively.

$$E_{p,a} = (1.282 \pm 0.004) - 0.00174T \quad (4)$$

$$E_{p,c} = (1.459 \pm 0.089) - 0.00224T \quad (5)$$

As the temperature rising, E_p shifted to the low potentials for both two samples, indicating the improved CO oxidation at high temperatures. However, the absolute slop value of -2.24 ± 0.28 mV K^{-1} for sample C is higher than that of -1.74 ± 0.01 mV K^{-1} for sample A, illustrating that temperature dependence of E_p is more remarkable for smaller platinum particles. From the intercept of the line, apparent activation energy (E_a) was calculated to be 123.7 ± 0.4

Table 2
The comparison for the trend of E_a and E_p between the reported Pt (1 1 1), Pt (1 0 0), and as-produced samples A and C

Sample	E_a (kJ mol^{-1})	E_p (V vs. SCE, 298 K)
Pt (1 1 1)	111[a]	0.47[b]
Pt (1 0 0)	122[a]	0.48[b]
A (4.0 nm)	124	0.516
C (1.7 nm)	141	0.562

[a] The value was reported in Ref. [16].
[b] The value was calculated from Ref. [16] in 0.1 M $HClO_4$ aqueous solution.

and 140.8 ± 8.6 kJ mol^{-1} for samples A and C, respectively. The values are higher than the reported 111 ± 5 kJ mol^{-1} for Pt (1 1 1) and 122 ± 5 kJ mol^{-1} for Pt (1 0 0) electrode [16]. For the sake of comparison, the values of E_a and the corresponding E_p (under the same temperature of 298 K) for samples A, C, Pt (1 1 1), and Pt (1 0 0) are listed in Table 2. Both E_p positions of Pt nanoparticles were observed higher than that of single crystal surface of Pt, suggesting that CO is adsorbed stronger on the nanoparticles than on the single crystal surfaces. Furthermore, E_a was found increased coherently with the positive shift of E_p. Those observations revealed that the nature of increased E_a reasonably resulted from their stronger adsorption of CO. Comparing to the CO diffusion process, studied of alumina supported Pt clusters using ^{13}C NMR by Sinfelt et al. [24], we summarized that both of the apparent E_a for CO_{ads} electrooxidation and activation energy for CO_{ads} diffusion (E_{diff}) increased as the size decreased, confirming the same fact that the adsorption of CO was stronger on the smaller Pt particles.

As discussed above, the reaction of CO electrooxidation on smaller Pt particles required higher overpotential and higher apparent E_a. However, MA of the catalysts A, B, and C towards methanol oxidation was found increased monotonically as the particle size decreased (in Fig. 9). The values were calculated to be ca. 620, 750, and 1050 mA mg^{-1} Pt, respectively. In our approach, the maximum of MA in methanol electrooxidation was reached by the catalyst with the smallest Pt particles in the particular size range of 1.7–4.0 nm, which was different from the results of Tang et al. [10], but was in line with the results of Frelink et al. [25] and Zeng et al. [11]. The following analysis proved that the trend of MA is not controversial to the results of CO-stripping. Considering the same support, same preparing method and similar high dispersion of Pt particles, such a maximum might be due to the enhanced active sites and the number of OH_{ads} per weight of Pt as the ESA increased. Assuming the increase of MA is proportional to the increase of ESA, the MA of catalyst C (1.7 nm) would be 2.8 times that of catalyst A (4.0 nm) instead of the observed ratio of 1.7 times. The discount of

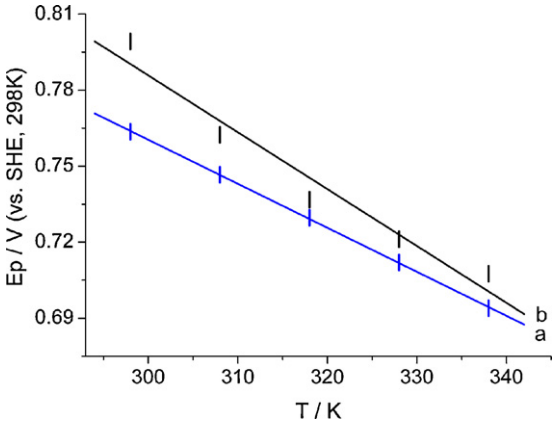

Fig. 8. The fit line of E_p vs. T for the electrodes of (a) sample A and (b) sample C.

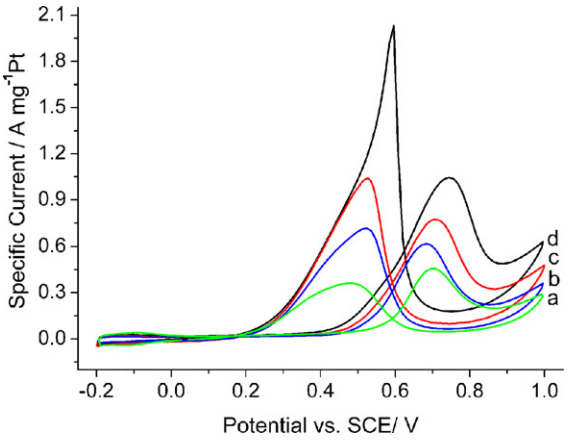

Fig. 9. The cyclic voltammetry curves of the (a) catalyst D, (b) catalyst A, (c) catalyst B, and (d) catalyst C for methanol electrooxidation in 1 M CH_3OH + 1 M $HClO_4$, 50 mV s^{-1}, 25 °C (the cyclic curves reached stable within 10 scans, only the 50th cycle ones are demonstrated).

MA increase for sample C indicates that the ESA is not the exclusive factor to the catalytic activities. It is reasonable due to a compromise between the size-effect induced two competitions: the improved utilization of smaller platinum particles against their stronger CO_{ads} adsorption. Apart from the deactivation of the increased amount of Pt^{II} species (5%, not active for methanol electrooxidation), the deactivation of MA for the smaller particles mainly results from their more intense CO-poisoning, which limits the beneficial influence in the higher mass activity in this case. Besides, MA of three samples A, B, and C was markedly higher than the value of benchmark Pt/C (sample D, 450 mA mg^{-1} Pt), confirming the beneficial role of MWCNT support.

Apart from the potentiodynamic investigation, the potentiostatic one is another measurement to study the catalyst performance in methanol electrooxidation, which can give clues about catalyst poisoning or stability loss [9]. The chronoamperometry tests were performed at the potential of 0.5 V for 3600 s, as demonstrated in Fig. 10. The currents were normalized by the weight of Pt. The potentiostatic currents decreased rapidly at the beginning for four catalysts, suggesting the accumulated poisoning of intermediate CO-like species during the methanol oxidation reaction [26,27]. After long time operation, the current decay slowed down. We attribute this to a semi-equilibrium reached between CO-poisoning and methanol oxidation on the anode at this stage. The decay of current is in the similar model for four catalysts

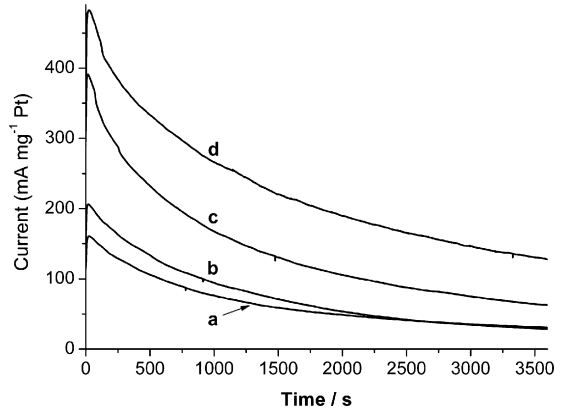

Fig. 10. The chronoamperometric curves of the (a) catalyst D, (b) catalyst A, (c) catalyst B, and (d) catalyst C for methanol electrooxidation in 1 M CH_3OH + 1 M $HClO_4$, 0.5 V vs. SCE, 25 °C.

Table 3
The comparison between MA and SA in the reactions of methanol, ethanol, and EG electrooxidation as the particle size of Pt decreased

Samples	Methanol electrooxidation			Ethanol electrooxidation		EG electrooxidation	
	ESA ($m^2\ g^{-1}$)	MA ($mA\ mg^{-1}$ Pt)	SA ($mA\ cm^{-2}$ Pt)	MA ($mA\ mg^{-1}$ Pt)	SA ($mA\ cm^{-2}$ Pt)	MA ($mA\ mg^{-1}$ Pt)	SA ($mA\ cm^{-2}$ Pt)
A	37.9	620	1.64	700	1.85	486	1.28
B	73.2	750	1.02	880	1.20	736	1.01
C	107	1050	0.98	1040	0.97	888	0.83

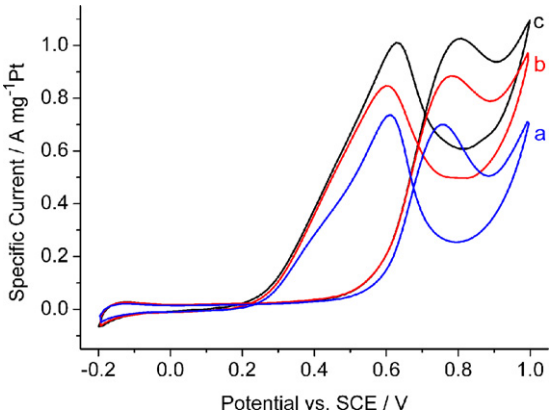

Fig. 11. The cyclic voltammetry curves of the (a) catalyst A, (b) catalyst B, and (c) catalyst C for ethanol electrooxidation in 1 M CH_3OH + 1 M $HClO_4$, 50 mV s^{-1}, 25 °C (the cyclic curves reached stable within 10 scans, the 50th cycle ones are demonstrated for comparison).

during the process going, however, the currents at the electrode of sample C were found to be the highest in the whole process, while the values for A and D were the lowest, indicating the high activity of the small particles under the same static potential. Those are in line with the CV results.

Considering that ethanol and ethylene glycol (EG) are less toxic than methanol, especially, EG is less pass through the polymer-exchange membrane (low crossover) [28], ethanol and EG are the appealing candidates to replace methanol as the fuel. The size-effect on MA in ethanol and EG electrooxidation was also investigated, as illustrated in Figs. 11 and 12. MA for both two processes were found increased as the Pt particle size decreased, which are very similar to the case of methanol oxidation, although the reactions (involving C–C breaking) are more complex. The maximum of MA was also reached by the catalyst C with the smallest particle size (1.7 nm). The results suggested that the reactions involving in ethanol and EG electrooxidation are also demanding

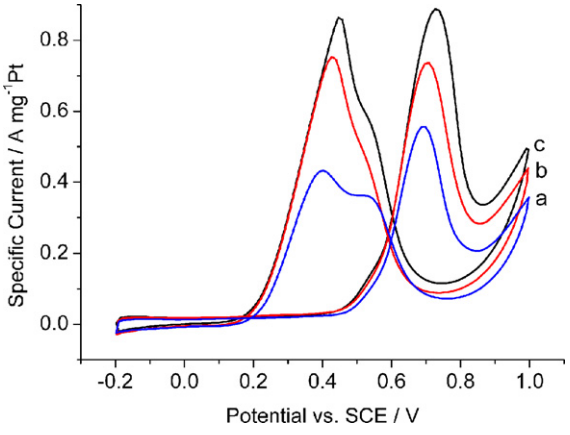

Fig. 12. Same as Fig. 11 but for ethylene glycol electrooxidation.

to the Pt particle size. Besides, it is noticeable that the peak potential for EG electrooxidation is at ca. 0.7 V, which is ca. 80 mV lower than that for ethanol electrooxidation. It is possibly attributed to the different oxidative route for two processes at 25 °C. The origin requires further investigation.

Apart from mass activity, the specific activity to methanol, ethanol, and EG electrooxidation was calculated and summarized in Table 3. The values of ESA and MA were listed for comparison. After subtracting the influence of ESA, SA was found decreased as the particle size decreased, which was opposite to the trend of MA. The high MA and low SA reflect the catalytic activities from different aspects for smaller platinum particles and are rationalized in our study. And the trend of SA was in line with the results of CO-stripping and could be explained by the restricted CO diffusion on smaller particles. SA is better to mirror the intrinsic nature of Pt particles.

The observed size-effect enlighten us to conclude that (1) we should pay attention to the particle size of Pt when we compare the catalyst activity directly with E_p shift in CO-stripping curves. It will be not valuable when the particle sizes of Pt are quite different. (2) High MA means that high current density and power output can be generated on per mass of Pt. The value of MA is not only the direct index but an indispensable aspect to evaluate the activity of catalysts in practical applications, especially considering the high cost of noble metal of Pt.

The study of size-effect on the catalyst performance in a single cell is underway in our lab.

4. Conclusions

The study in this paper demonstrates a strong activity dependence on their particle size towards CO and alcohol electrooxidation reactions.

(1) The reaction of CO electrooxidation was found occurring at higher overpotential and higher apparent activation energy on the smaller Pt nanoparticles than on the larger ones. The nature of those observed phenomena are due to their stronger CO adsorption.
(2) The MA towards the reaction of alcohol electrooxidation was observed increased as platinum particles decreased. The improved MA can be reasonably attributed to the improved utilization of Pt particles as well as the enhanced amount of OH_{ads} formed per weight of Pt. Considering the discount of MA increase, we conclude that the deactivation of MA for the smaller particles arises from their stronger CO adsorption, which limited their beneficial effect on the higher mass activity in this case. Therefore, the trend of MA is not controversial to the results of CO-stripping. Consequently, we should pay attention to the particle size of Pt when we evaluate the performance of Pt-based catalysts directly by E_p shift in CO-stripping curves. It will lead to some misunderstanding when the particle sizes of Pt are quite different.
(3) The decreased SA for the smaller platinum particles was found in line with the results of CO-stripping, and could be explained by the restrict CO diffusion. This indicates that SA is more

helpful in qualitative characterizing the intrinsic nature of the catalysts.

(4) Taking into account of the high cost of noble metal of Pt, the value of MA is an indispensable aspect to evaluate their catalytic activities in practical applications. The small Pt nanoparticles can increase the utilization of Pt and their MA, meanwhile, reduce the loading of platinum. Hence, the small platinum nanoparticles enclosed by high-index planes are expected to be a new orientation to further improve the performance of Pt-based catalysts.

Acknowledgements

The work is financially supported by the State Key Basic Research Program of PRC (2002CB211803), Natural Science Foundation of Beijing (2051001), and China Postdoctoral Science foundation (20060400459).

References

[1] H.S. Liu, C.J. Song, L. Zhang, J.J. Zhang, H.J. Wang, D.P. Wilkinson, J. Power Sources 155 (2006) 95–110.
[2] V. Baglio, A. Di Blasi, E. Modica, P. Cretì, V. Antonucci, A.S. Aricò, J. New Mater. Electrochem. Syst. 9 (2006) 41–46.
[3] L. Cao, F. Scheiba, C. Roth, F. Schweiger, C. Cremers, U. Stimming, H. Fuess, L.Q. Chen, W.T. Zhu, X.P. Qiu, Angew. Chem. Int. Ed. 45 (2006) 5315–5319.
[4] C.A. Bessel, K. Laubernds, N.M. Rodriguez, R.T.K. Baker, J. Phys. Chem. B 105 (2001) 1115–1118.
[5] G. Girishkumar, T.D. Hall, K. Vinodgopal, P.V. Kamat, J. Phys. Chem. B 110 (2006) 107–114.
[6] N. Tian, Z.Y. Zhou, S.G. Sun, Y. Ding, Z.L. Wang, Science 316 (2007) 732–735.
[7] F. Maillard, M. Eikerling, O.V. Cherstiouk, S. Schreier, E. Savinova, U. Stimming, Faraday Discuss. 125 (2004) 357–377.
[8] M. Arenz, K.J.J. Mayrhofer, V. Stamenkovic, B.B. Blizanac, T. Tomoyuki, P.N. Ross, N.M. Markovic, J. Am. Chem. Soc. 127 (2005) 6819–6829.
[9] K. Bergamaski, A.L.N. Pinheiro, E. Teixeira-Neto, F.C. Nart, J. Phys. Chem. B 110 (2006) 19271–19279.
[10] Y.W. Tang, L.L. Zhang, Y.N. Wang, Y.M. Zhou, Y. Gao, C.P. Liu, W. Xing, T.H. Lu, J. Power Sources 162 (2006) 124–131.
[11] J.H. Zeng, J.Y. Lee, W.J. Zhou, Appl. Catal. A: Gen. 308 (2006) 99–104.
[12] Y.B. Wang, Z. Iqbal, S. Mitra, J. Am. Chem. Soc. 128 (2006) 95–99.
[13] C. Bock, C. Paquet, M. Couillard, G.A. Botton, B.R. MacDougall, J. Am. Chem. Soc. 126 (2004) 8028–8037.
[14] C. Bock, B. MacDougall, J. Electrochem. Soc. 150 (2003) E377–E383.
[15] F. Scheibal, M. Scholz, L. Cao, R. Schafranek, C. Roth, C. Cremers, X.P. Qiu, U. Stimming, H. Fuess, Fuel Cells 6 (2006) 439–446.
[16] E. Herrero, J.M. Feliu, S. Blais, Z. Radovic-Hrapovic, G. Jerkiewicz, Langmuir 16 (2000) 4779–4783.
[17] C. Susut, T.D. Nguyen, G.B. Chapman, Y.Y. Tong, J. Cluster Sci. 18 (2007) 773–780.
[18] A. Pozio, M.D. Francesco, A. Cemmi, F. Cardellini, L. Giorgi, J. Power Sources 105 (2002) 13–19.
[19] Y. Takasij, N. Ohashi, X.G. Zhang, Y. Murakami, H. Minagawa, S. Sato, K. Yahikozawa, Electrochim. Acta 41 (1996) 2595–2600.
[20] H.A. Gasteiger, N. Marković, P.N. Ross, E.J. Cairns, J. Phys. Chem. 97 (1993) 12020–12029.
[21] S. Mukerjee, J. McBreen, J. Electroanal. Chem. 448 (1998) 163–171.
[22] T. Kawaguchi, W. Sugimoto, Y. Murakami, Y. Takasu, Electrochem. Commun. 6 (2004) 480–483.
[23] E. Herrero, B. Alvarez, J.M. Feliu, S. Blais, Z. Radovic-Hrapovic, G. Jerkiewicz, J. Electroanal. Chem. 567 (2004) 139–149.
[24] L.R. Becerra, C.A. Klug, C.P. Slichter, J.H. Sinfelt, J. Phys. Chem. 97 (1993) 12014.
[25] T. Frelink, W. Visscher, J.A.R. van Veen, J. Electroanal. Chem. 382 (1995) 65– 72.
[26] A. Kabbabi, R. Faure, R. Durand, B. Beden, F. Hahn, J.M. Leger, C. Lamy, J. Electroanal. Chem. 444 (1998) 41–53.
[27] J. Prabhuram, T.S. Zhao, Z.K. Tang, R. Chen, Z.X. Liang, J. Phys. Chem. B 110 (2006) 5245–5252.
[28] V. Livshits, E. Peled, J. Power Sources 161 (2006) 1187–1191.